This is the accepted manuscript made available via CHORUS. The article has been published as:

Anisotropic neutron spin resonance in underdoped superconducting NaFe_{1−x}Co_{x}As

Chenglin Zhang, Yu Song, L.-P. Regnault, Yixi Su, M. Enderle, J. Kulda, Guotai Tan, Zachary C. Sims, Takeshi Egami, Qimiao Si, and Pengcheng Dai

Phys. Rev. B **90**, 140502 — Published 1 October 2014

DOI: 10.1103/PhysRevB.90.140502

Anisotropic neutron spin resonance in underdoped superconducting $NaFe_{1-x}Co_xAs$

Chenglin Zhang,[1,2,*] Yu Song,[1,*] L.-P. Regnault,[3] Yixi Su,[4] M. Enderle,[5] J. Kulda,[5]
Guotai Tan,[2] Zachary C. Sims,[2] Takeshi Egami,[2,6] Qimiao Si,[1] and Pengcheng Dai[1,†]

[1]*Department of Physics and Astronomy, Rice University, Houston, Texas 77005, USA*
[2] *Department of Physics and Astronomy, The University of Tennessee, Knoxville, Tennessee 37996-1200, USA*
[3]*SPSMS-MDN, UMR-E CEA/UJF-Grenoble 1, INAC, Grenoble, F-38054, France*
[4] *Jülich Centre for Neutron Science, Forschungszentrum Jülich GmbH, Outstation at MLZ, D-85747 Garching, Germany*
[5]*Institut Laue-Langevin, 6, rue Jules Horowitz, BP 156, 38042 Grenoble Cedex 9, France*
[6]*Oak Ridge National Laboratory, Oak Ridge, Tennessee 37831, USA*

(Dated: September 18, 2014)

We use polarized inelastic neutron scattering (INS) to study spin excitations in superconducting $NaFe_{0.985}Co_{0.015}As$ (C15) with static antiferromagnetic (AF) order along the a-axis of the orthorhombic structure and $NaFe_{0.935}Co_{0.045}As$ (C45) without AF order. In previous unpolarized INS work, spin excitations in C15 were found to have a dispersive sharp resonance near $E_{r1} = 3.25$ meV and a broad dispersionless mode at $E_{r2} = 6$ meV. Our neutron polarization analysis reveals that the dispersive resonance in C15 is highly anisotropic and polarized along the a- and c-axis, while the dispersionless mode is isotropic similar to that of C45. Since the a-axis polarized spin excitations of the anisotropic resonance appear below T_c, our data suggests that the itinerant electrons contributing to the magnetism are also coupled to the superconductivity.

PACS numbers: 74.70.Xa, 75.30.Gw, 78.70.Nx

Superconductivity in iron pnictides occurs when the antiferromagnetic (AF) order in their parent compounds is suppressed via electron or hole-doping [1–7]. In the undoped state, iron pnictides exhibit a tetragonal to orthorhombic lattice distortion at temperature T_s, followed by a paramagnetic to AF phase transition at T_N with a collinear AF structure and the ordered moments along the a-axis of the orthorhombic lattice [inset in Fig. 1(a) or M_a] [1–7]. Upon doping to induce superconductivity, the most prominent feature in the spin excitations spectrum is a neutron spin resonance arising below T_c at the in-plane AF ordering wave vector $\mathbf{Q_{AF}} = (1, 0)$ [8–14]. For hole and electron-doped $BaFe_2As_2$ family of materials [8–14], the resonance occurs at an energy E believed to be associated with the superconducting gap energies at the hole and electron Fermi surfaces near Γ and M points in the reciprocal space, respectively [15]. In the case of electron-doped superconducting $NaFe_{1-x}Co_xAs$ [Fig. 1(a)] [16–18], unpolarized inelastic neutron scattering (INS) experiments reveal that superconductivity induces a dispersive sharp resonance near $E_{r1} = 3.25$ meV and a broad dispersionless mode at $E_{r2} = 6$ meV at $\mathbf{Q_{AF}} = (1, 0)$ in the underdoped $NaFe_{0.985}Co_{0.015}As$ (C15) with static AF order ($T_c = 15$ K and $T_N = 30$ K) [19], while only a single resonance at $E_r = 7$ meV in the overdoped $NaFe_{0.935}Co_{0.045}As$ (C45, $T_c = 18$ K) [20].

The presence of double resonance in superconducting C15 coexisting with static AF order [19] has inspired much discussion on its microscopic origin. In one class of models, the double resonance arises from superconductivity coexisting with static AF order [21, 22]. In this picture, through an averaging effect in twinned samples, the double resonances observed at, say, $\mathbf{Q} = (1, 0)$, are interpreted as reflecting one single resonance at the AF zone center $\mathbf{Q_{AF}} = (1, 0)$ and one at the wave vector $\mathbf{Q}' = (0, 1)$ [21, 22]. Alternatively, the double resonance in C15 may probe the superconducting gap anisotropy in the underdoped regime seen in the angle resolved photoemission experiments [19, 23, 24]. Here, the orbital-selective pairing gives rise to gap anisotropy along a Fermi surface with hybridized orbital characters, resulting a split of the neutron spin resonance [24]. Since the resonance is generally believed to result from a triplet excitation of the singlet electron Cooper pairs associated with isotropic paramagnetic spin excitations [$M_a = M_b = M_c$ in the inset of Fig. 1(a)] [25], a determination of its spatial anisotropy is important for understanding the double resonance and its microscopic origin.

In this paper, we report polarized INS studies of undoped C15 and overdoped C45 [19, 20]. We find that the dispersive resonance in C15 is highly anisotropic and polarized along the a- and c-axis ($M_a, M_c > 0$) with no contribution from the b-axis ($M_b = 0$). However, the dispersionless resonances in C15 and C45 are isotropic with ($M_a = M_b = M_c$), consistent with the singlet-to-triplet excitations [25]. Since spin waves in the undoped NaFeAs are entirely c-axis polarized for energies below $\sim$10 meV [26], the appearance of a-axis (longitudinally) polarized resonance in the AF ordered C15 below T_c indicates that the dispersive resonance is unlikely to arise from coexisting AF order with superconductivity [21, 22]. Instead, the data is consistent with the orbit-selective superconducting gap anisotropy [24], suggesting that the itinerant electron contributions to the magnetism, revealed as longitudinal spin excitations in undoped parent compounds

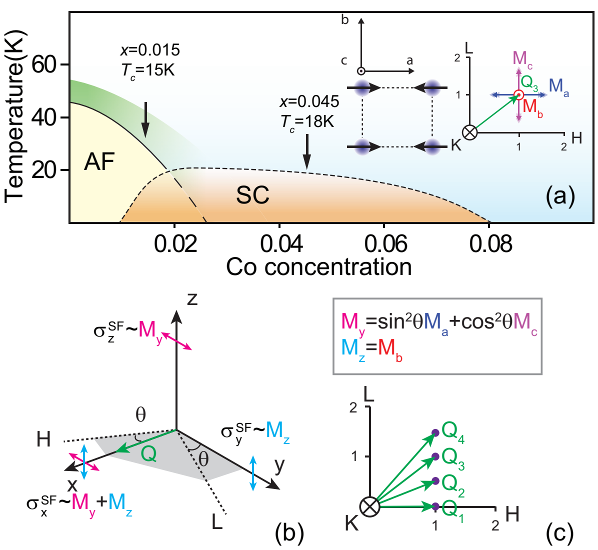

FIG. 1: (Color online) (a) The phase diagram of $NaFe_{1-x}Co_xAs$ with $x = 0.015, 0.045$ marked by vertical arrows [16]. The left inset shows the orthorhombic unit cell of NaFeAs with the arrows indicating directions of the ordered moments. The right inset shows reciprocal space in the $[H, 0, L]$ scattering plane. The blue, red, and purple arrows mark spin excitations along the M_a, M_b, and M_c directions, respectively. (b) The relationship between the neutron polarization directions (x, y, z) and the probed reciprocal space. The angle between x-direction and the H-axis is denoted as θ. $\sigma_x^{\rm SF}$ contains both M_y and M_z magnetic components, whereas only M_y and M_z contribute to $\sigma_z^{\rm SF}$ and $\sigma_y^{\rm SF}$, respectively. (c) The $\mathbf{Q_1} = (1, 0, 0)$, $\mathbf{Q_2} = (1, 0, 0.5)$, $\mathbf{Q_3} = (1, 0, 1)$, $\mathbf{Q_4} = (1, 0, 1.5)$ mark the probed reciprocal space.

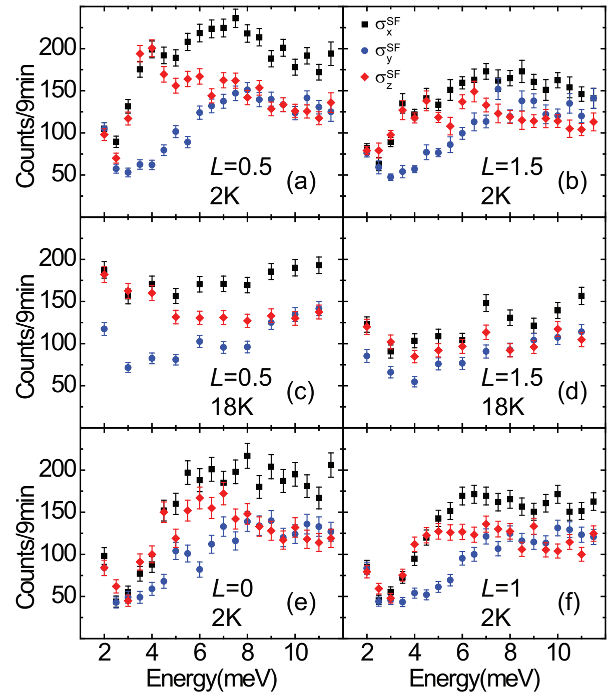

FIG. 2: (Color online) Neutron spin-flip scattering $\sigma_x^{\rm SF}$, $\sigma_y^{\rm SF}$, and $\sigma_z^{\rm SF}$ at (a) $\mathbf{Q_2}$ (b) $\mathbf{Q_4}$ in the superconducting state. (c,d) Identical scans in the normal state. (e,f) $\sigma_x^{\rm SF}$, $\sigma_y^{\rm SF}$, and $\sigma_z^{\rm SF}$ at $\mathbf{Q_1}$ and $\mathbf{Q_3}$, respectively.

[27], are also coupled to superconductivity.

The inset in Fig. 1(a) shows the AF structure of NaFeAs with orthorhombic lattice parameters $a = 5.589$, $b = 5.569$ and $c = 6.991$ Å [4]. We define momentum transfer $\mathbf{Q}$ in three-dimensional reciprocal space in Å^{-1} as $\mathbf{Q} = H\mathbf{a}^* + K\mathbf{b}^* + L\mathbf{c}^*$, where H, K, and L are Miller indices and $\mathbf{a}^* = \hat{\mathbf{a}}2\pi/a$, $\mathbf{b}^* = \hat{\mathbf{b}}2\pi/b$, $\mathbf{c}^* = \hat{\mathbf{c}}2\pi/c$. In this notation, the AF Bragg peaks and zone centers occur at $[1, 0, L]$ with $L = 0.5, 1.5, \cdots$, while the AF zone boundaries along the c-axis occur at $L = 0, 1, 2, \cdots$ [4]. The dynamic susceptibility along the a-, b-, and c-axis directions corrected for the Bose population factor are marked as M_a, M_b, and M_c, respectively [inset in Fig. 1(a)] [28]. Our polarized INS experiments were carried out using the IN20 and IN22 triple-axis spectrometers at the Institut Laue-Langevin, Grenoble, France [26–31]. Single crystals of C14 and C45 used in previous unpolarized neutron scattering experiments are used in the present experiment [19, 20]. The quality of our single crystals of $NaFe_{1-x}Co_xAs$ has been reported in previous heat capacity [18], angle resolved photoemission spectroscopy [23], and nuclear magnetic resonance [32, 33] experiments. We define the neutron polarization directions along $\mathbf{Q}$ as x, perpendicular to $\mathbf{Q}$ but in the scattering plane as y, and perpendicular to $\mathbf{Q}$ and the scattering plane as z, respectively [Figs. 1(b)]. At wave vector $\mathbf{Q}$, one can probe magnetic responses within the $y-z$ plane (M_y and M_z), giving $M_y = M_a \sin^2\theta + M_c \cos^2\theta$ and $M_z = M_b$, where the angle between $\mathbf{Q}$ and $[H, 0, 0]$ is θ [Fig. 1(b)] [28]. By probing two or more equivalent AF wave vectors with different angle θ, we can conclusively determine M_a, M_b, and M_c (Fig. 1c) [26].

To establish the spin excitation anisotropy in $NaFe_{1-x}Co_xAs$, we carried out polarized INS in C15 [19]. Figures 2(a) and 2(b) show neutron spin-flip (SF) scattering for neutron polarizations along the x ($\sigma_x^{\rm SF}$), y ($\sigma_y^{\rm SF}$), and z ($\sigma_z^{\rm SF}$) directions at the AF zone centers $\mathbf{Q_2} = \mathbf{Q_{AF}} = (1, 0, 0.5)$ and $\mathbf{Q_4} = (1, 0, 1.5)$, respectively, in the superconducting state ($T = 2$ K). We find that $\sigma_x^{\rm SF}$ has a narrow peak at $E_{r1} \approx 4$ meV and a broad peak at $E_{r2} = 7$ meV, consistent with the two resonances in previous unpolarized work [19]. However, the situation is rather different for $\sigma_y^{\rm SF} \sim M_z = M_b$ and $\sigma_z^{\rm SF} \sim M_y$. While $\sigma_z^{\rm SF}$ has clear peaks at $E_{r1} \approx 4$ and $E_{r2} = 7$ meV, $\sigma_y^{\rm SF}$ has a broad peak at $E_{r2} = 7$ meV and is featureless at $E_{r1} \approx 4$ meV. Identical scans in the normal state ($T = 18$ K) reveal magnetic anisotropy below 8 meV with $\sigma_x^{\rm SF} \geq \sigma_z^{\rm SF} > \sigma_y^{\rm SF}$ [Figs. 2(c) and 2(d)]. Figures 2(e) and 2(f) show similar data at the AF zone boundaries $\mathbf{Q_1} = (1, 0, 0)$ and $\mathbf{Q_3} = (1, 0, 1)$, respectively, in the superconducting state.

Using data in Fig. 2, we determine the magnetic

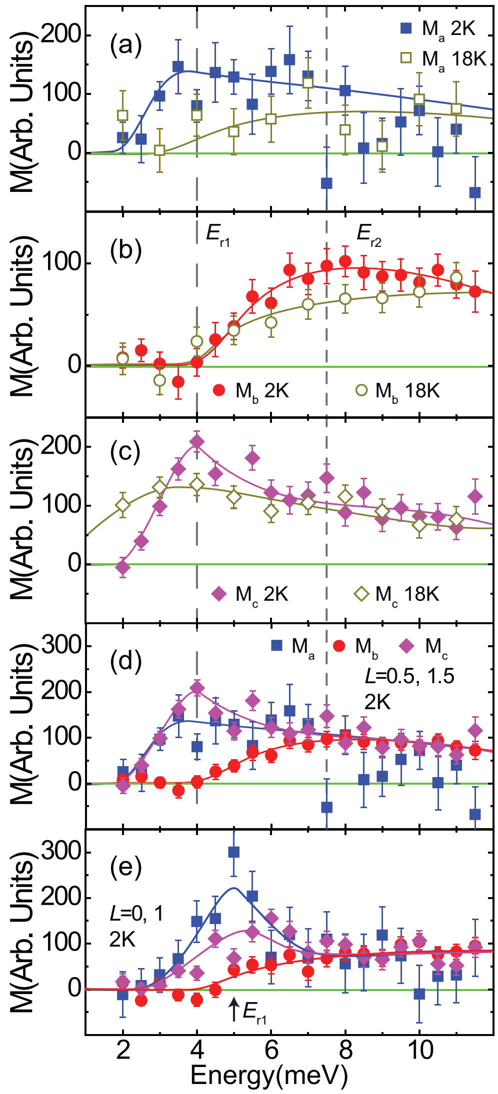

FIG. 3: (Color online) Energy dependence of the dynamic susceptibility (a) M_a, (b) M_b, and (c) M_c above and below T_c. Energy dependence of M_a, M_b, M_c in the superconducting state at (d) AF zone center and (e) zone boundary. The vertical dashed lines indicate energies of E_{r1} and E_{r2}, and the solid lines are guides to the eye.

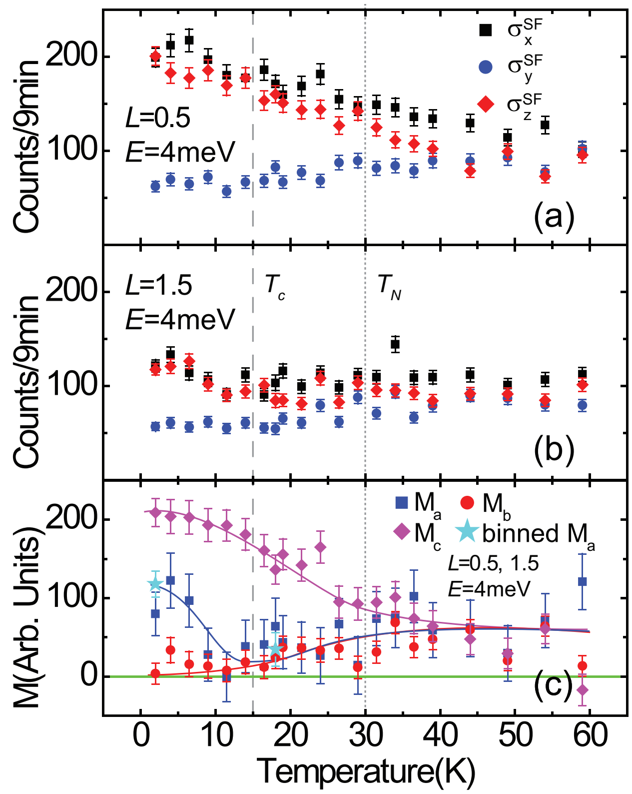

FIG. 4: (Color online) Temperature dependence of σ_x^{SF}, σ_y^{SF}, and σ_z^{SF} at $E = 4$ meV and (a) $\mathbf{Q_{AF}} = \mathbf{Q_2} = (1, 0, 0.5)$, (b) $\mathbf{Q_{AF}} = \mathbf{Q_4} = (1, 0, 1.5)$. (c) Temperature dependence of the estimated M_a, M_b, and M_c at $E = 4$ meV. The stars below and above T_c are from binned energy scan data near $E = 4$ meV. The vertical dashed lines mark T_N and T_c. The solid lines are guides to the eye.

anisotropy M_a, M_b, and M_c in C15 [34]. Figures 3(a), 3(b), and 3(c) show energy dependence of the M_a, M_b, and M_c, respectively, above and below T_c. While spin excitations along the M_a and M_c directions show clear peaks in the superconducting state above the normal state scattering near $E_{r1} \approx 4$ meV [Figs. 3(a) and 3(c)], there are no detectable difference in M_b across T_c at $E_{r1} \approx 4$ meV [Fig. 3(b)]. In contrast, spin excitations along the b-axis direction (M_b) show the most dramatic change below T_c near $E_{r2} \approx 7$ meV. Figure 3(d) plots the energy dependence of the M_a, M_b, and M_c in the superconducting state, showing a large spin gap below $\sim$4 meV and isotropic paramagnetic scattering above $\sim$7 meV. Therefore, the resonance at $E_{r1} \approx 4$ meV is composed of spin excitations polarized along the a (M_a) and c (M_c) axes, while the mode at $E_{r2} = 7$ meV is isotropic in space with $M_a \approx M_b \approx M_c$. Figure 3(e) shows the energy dependence of M_a, M_b, and M_c in the superconducting state at the AF zone boundary $\mathbf{Q_1} = (1, 0, 0)$. Consistent with unpolarized INS work [19], we find that the resonance at $E_{r1} \approx 4$ meV shifted up in energy to $E_{r1} \approx 5$ meV while the broad resonance remains unchanged at $E_{r2} \approx 7$ meV. Similar to the data at the AF zone center, the resonance at $E_{r1} \approx 5$ meV has M_a and M_c components with $M_b = 0$ and spin excitations are isotropic for energies above 7 meV.

Since the resonance at the AF zone center shows clear magnetic anisotropy in the superconducting state, we carried out temperature dependent measurements of the spin-flip scattering at $E_{r1} \approx 4$ meV. Figure 4(a) and 4(b) shows the $\sigma_x^{\rm SF}$, $\sigma_y^{\rm SF}$, and $\sigma_z^{\rm SF}$ scattering at the AF wave vectors $\mathbf{Q_2} = (1, 0, 0.5)$ and $\mathbf{Q_4} = (1, 0, 1.5)$, respectively. In previous unpolarized measurements, temperature dependence of the scattering at $E_{r1} = 3.25$ meV reveals a kink at $T_N \approx 30$ K and a clear enhancement below

$T_c = 15$ K [19]. Figure 4(c) shows temperature dependence of the M_a, M_b and M_c obtained by using data in Figs. 4(a) and 4(b). In the paramagnetic state, spin excitations are isotropic with $M_a = M_b = M_c$. On cooling to below T_N, spin excitations are dominated by c-axis polarized moment M_c with rapid suppression of M_a and M_b. These results are consistent with previous polarized INS work that show entirely c-axis polarized low-energy spin waves (M_c) in the AF ordered state of NaFeAs [26]. While M_c continues to increase with decreasing temperature and shows no obvious anomaly across T_c, M_a increases dramatically below T_c similar to the superconducting order parameter. In contrast, there are no b-axis polarized magnetic scattering below T_c ($M_b = 0$).

Having established the spin excitation anisotropy in electron underdoped C15 with static AF order and double resonances [19], it would be interesting to determine what happens in electron-overdoped C45, which has no static AF order and a sharp resonance at $E_r = 7$ meV [20]. From polarized INS data presented in [34], we conclude that magnetic scattering in electron overdoped C45 is isotropic at all energies and temperatures with $M_a = M_b = M_c$.

In previous polarized INS work on the parent compound $BaFe_2As_2$, spin waves below $\sim$12 meV are entirely c-axis polarized (M_c) [27, 35]. Upon electron-doping to $BaFe_2As_2$ via Co substitution to induce optimal superconductivity, polarized INS found evidence for two neutron spin resonance-like excitations with one isotropic mode ($M_a = M_b = M_c$) at an energy of $\sim$8 meV and a purely c-axis polarized mode (M_c) at $\sim$4 meV [36]. These results suggest that the low-energy c-axis polarized mode arises from the c-axis polarized spin waves in the parent compound [36]. The discovery that the $E_{r1} = 3.25$ meV sharp resonance in the underdoped Co15 is composed of a primarily longitudinally polarized mode coupled to superconductivity is clearly different from those of electron-doped $BaFe_2As_2$ superconductors [31, 36]. Since the c-axis polarized excitations of the $E_{r1} = 3.25$ meV resonance shows no anomaly across T_c in the C15 [M_c in Fig. 4(c)] and its spin anisotropy features at the AF zone boundary along the c-axis [$L = 0, 1$, Fig. 3(e)] are rather similar to those at the zone center [$L = 0.5, 1.5$, Fig. 3(d)], the mode is unlikely to arise from the c-axis polarized spin waves coupling with superconductivity [21, 22]. By contrast, these observations are consistent with the scenario based on orbit-selectivity-induced superconducting gap anisotropy [24]. In this latter picture, the anisotropy of the spin resonance arises from a spin-orbit coupling, which operates when the resonance comes from the superconducting quasiparticle-quasihole excitations that are associated with both the $3d$ xy and xz/yz orbitals [24].

To summarize, our discovery of a primarily longitudinally polarized resonance at $E_{r1} \approx 4$ meV implies that the longitudinal spin excitations typically associated with magnetism from itinerant electrons are also coupled to superconductivity. This suggests that itinerant electrons play an important role in the low-energy spin dynamics of the superconducting state. At the same time, our study provides further evidence for the role of electron-correlation-induced orbital selectivity in the superconducting state, underscoring the importance of the local correlations to the superconducting resonance excitations. Taken together, our results indicate that even the nominally itinerant-electron contributions to the low-energy spin excitations encode the effects of local electronic correlations. This is a new insight in the microscopic physics of the iron-pnictide superconductors.

We thank useful discussions with Weicheng Lv, ilya Eremin and Rong Yu. The crystal growth and neutron scattering work at Rice/UTK was supported by the US DOE, BES, DE-FG02-05ER46202 (P.D.). Work at Rice University was supported by the NSF Grant No. DMR-1309531 (Q.S.) and the Robert A. Welch Foundation Grant Nos. C-1839 (P.D.) and C-1411 (Q.S.). C.L.Z and T.E are partially supported by the US DOE BES through the EPSCoR grant, DE-FG02-08ER46528.

* These authors made equal contributions to this paper
† Electronic address: pdai@rice.edu

[1] Y. Kamihara, T. Watanabe, M. Hirano, and H. Hosono, J. Am. Chem. Soc. **130**, 3296-3297 (2008).
[2] C. de la Cruz, Q. Huang, J. W. Lynn, J. Y. Li, W. Ratcliff II, J. L. Zarestky, H. A. Mook, G. F. Chen, J. L. Luo, N. L. Wang, and P. C. Dai, Nature (London) **453**,899 (2008).
[3] C. W. Chu, F. Chen, M. Gooch, A.M. Guloy, B. Lorenz, B. Lv, K. Sasmal, Z. J. Tang, J. H. Tapp, Y. Y. Xue, Physica C **469**, 326 (2009).
[4] S. L. Li, C. de la Cruz, Q. Huang, G. F. Chen, T.-L. Xia, J. L. Luo, N. L. Wang, and P. C. Dai, Phys. Rev. B **80**, 020504(R) (2009).
[5] Y. Song, S. V. Carr, X. Y. Lu, C. L. Zhang, Z. C. Sims, N. F. Luttrell, S. Chi, Y. Zhao, J. W. Lynn, P. C. Dai, Phys. Rev. B **87**, 184511 (2013).
[6] D. C. Johnston, Advances in Physics **59**, 803 (2010).
[7] P. C. Dai, J. P. Hu, and E. Dagotto, Nature Phys. **8**, 709 (2012).
[8] A. D. Christianson, E. A. Goremychkin, R. Osborn, S. Rosenkranz, M. D. Lumsden, C. D. Malliakas, I. S. Todorov, H. Claus, D. Y. Chung, M. G. Kanatzidis, R. I. Bewley, and T. Guidi, Nature (London) **456**, 930 (2008).
[9] M. D. Lumsden, A. D. Christianson, D. Parshall, M. B. Stone, S. E. Nagler, G. J. MacDougall, H. A. Mook, K. Lokshin, T. Egami, D. L. Abernathy, E. A. Goremychkin, R. Osborn, M. A. McGuire, A. S. Sefat, R. Jin, B. C. Sales, and D. Mandrus, Phys. Rev. Lett. **102**, 107005 (2009).
[10] S. Chi, A. Schneidewind, J. Zhao, L. W. Harriger, L. Li, Y. Luo, G. Cao, Zhuan Xu, M. Loewenhaupt, J. Hu, and P. Dai, Phys. Rev. Lett. **102**, 107006 (2009).
[11] D. S. Inosov, J. T. Park, P. Bourges, D. L. Sun, Y.

Sidis, A. Schneidewind, K. Hradil, D. Haug, C. T. Lin, B. Keimer, and V. Hinkov, Nat. Phys. **6**, 178 (2010).
[12] C. H. Lee, P. Steffens, N. Qureshi, M. Nakajima, K. Kihou, A. Iyo, H. Eisaki, and M. Braden, Phys. Rev. Lett. **111**, 167002 (2013).
[13] M. G. Kim, G. S. Tucker, D. K. Pratt, S. Ran, A. Thaler, A. D. Christianson, K. Marty, S. Calder, A. Podlesnyak, S. L. Bud'ko, P. C. Canfield, A. Kreyssig, A. I. Goldman, and R. J. McQueeney, Phys. Rev. Lett. **110**, 177002 (2013).
[14] D. S. Inosov, J. T. Park, A. Charnukha, Yuan Li, A. V. Boris, B. Keimer, and V. Hinkov, Phys. Rev. B **83**, 214520 (2011).
[15] P. J. Hirschfeld, M. M. Korshunov, and I. I. Mazin, Rep. Prog. Phys. **74**, 124508 (2011).
[16] D. R. Parker, M. J. P. Smith, T. Lancaster, A. J. Steele, I. Franke, P. J. Baker, F. L. Pratt, M. J. Pitcher, S. J. Blundell, and S. J. Clarke et al., Phys. Rev. Lett. **104**, 057007 (2010).
[17] A. F. Wang, X. G. Luo, Y. J. Yan, J. J. Ying, Z. J. Xiang, G. J. Ye, P. Cheng, Z. Y. Li, W. J. Hu, and X. H. Chen, Phys. Rev. B **85**, 224521 (2012).
[18] G. T. Tan, P. Zheng, X. C. Wang, Y. C. Chen, X. T. Zhang, J. L. Luo, T. Netherton, Y. Song, P. C. Dai, C. L. Zhang, and S. L. Li, Phys. Rev. B **87**, 144512 (2013).
[19] C. L. Zhang, R. Yu, Y. X. Su, Y. Song, M. Y. Wang, G. T. Tan, T. Egami, J. A. Fernandez-Baca, E. Faulhaber, Q. Si, and P. C. Dai, Phys. Rev. Lett. **111**, 207002 (2013).
[20] C. L. Zhang *et al.*, Phys. Rev. B **88**, 064504 (2013).
[21] W. Rowe, J. Knolle, I. Eremin, and P. J. Hirschfeld, Phys. Rev. B **86**, 134513 (2012).
[22] W. C. Lv, A. Moreo, and E. Dagotto, Phys. Rev. B **89**, 104510 (2014).
[23] Q.Q. Ge, Z.R. Ye, M. Xu, Y. Zhang, J. Jiang, B.P. Xie, Y. Song, C.L. Zhang, P.C. Dai, and D.L. Feng, Phys. Rev. X **3**, 011020 (2013).
[24] R. Yu, J. X. Zhu, and Q. Si, Phys. Rev. B **89**, 024509 (2014).
[25] M. Eschrig, Adv. Phys. **55**, 47 (2006).
[26] Y. Song, L.-P. Regnault, C. L. Zhang, G. T. Tan, S. V. Carr, S. Chi, A. D. Christianson, T. Xiang, and P. C. Dai, Phys. Rev. B **88**, 134512 (2013).
[27] C. Wang, R. Zhang, F. Wang, H. Q. Luo, L. P. Regnault, P. C. Dai, and Y. Li, Phys. Rev. X **3**, 041036 (2013).
[28] O. J. Lipscombe, L. W. Harriger, P. G. Freeman, M. Enderle, C. L. Zhang, M. Y. Wang, T. Egami, J. P. Hu, T. Xiang, M. R. Norman, and P. C. Dai, Phys. Rev. B **82**, 064515 (2010).
[29] P. Babkevich, B. Roessli, S. N. Gvasaliya, L.-P. Regnault, P. G. Freeman, E. Pomjakushina, K. Conder, and A. T. Boothroyd, Phys. Rev. B **83**, 180506(R) (2011).
[30] K. Prokeš, A. Hiess, W. Bao, E. Wheeler, S. Landsgesell, and D. N. Argyriou, Phys. Rev. B **86**, 064503 (2012).
[31] H. Q. Luo, M. Wang, C. L. Zhang, X. Y. Lu, L.-P. Regnault, R. Zhang, S. L. Li, J. P. Hu, and P. C. Dai, Phys. Rev. Lett. **111**, 107006 (2013).
[32] S. Oh, A. M. Mounce, J. A. Lee, W. P. Halperin, C. L. Zhang, S. Carr, P. C. Dai, A. P. Reyes, and P. L. Kuhns, Phys. Rev. B **88**, 134518 (2013).
[33] S. Oh, A. M. Mounce, J. A. Lee, W. P. Halperin, C. L. Zhang, S. Carr, and P. C. Dai, Phys. Rev. B **87**, 174517 (2013).
[34] See supplementary material for details on how to estimate instrumentation effect at two equivalent wave vectors.
[35] N. Qureshi, P. Steffens, S. Wurmehl, S. Aswartham, B. Büchner, and M. Braden, Phys. Rev. B **86**, 060410(R) (2012).
[36] P. Steffens, C. H. Lee, N. Qureshi, K. Kihou, A. Iyo, H. Eisaki, and M. Braden, Phys. Rev. Lett. **110**, 137001 (2013).